Geochemical Perspectives Letters

Abiotic formation of organic biomorphs under diagenetic conditions

I. Criouet[1], J.-C. Viennet[1], P. Jacquemot[1,2], M. Jaber[2], S. Bernard[1*]

OPEN ACCESS

doi: 10.7185/geochemlet.2102

Abstract

The most ancient fossil record contains fundamentally important information on both the diversity and disparity of ancient life. Yet this ancient record is not that easy to decode, due to difficulties mainly pertaining to the impact of the geological history. Thus, the convergence of multiple lines of evidence is seen as necessary to build a robust demonstration of the biogenicity of putative traces of life. Yet, we experimentally show here that abiotic organic cell-like microstructures meeting all the criteria of biogenicity may form in cherts under classical conditions of diagenesis. These organic biomorphs produced from a mixture of RNA and quartz in water exposed to temperature and pressure conditions (200 °C, ~15 bars) exhibit morphological, chemical and isotopic signatures typical of organic microfossils. The results of this study exemplify the pitfalls that Archean palaeontologists may encounter when searching for traces of life in ancient rocks.

Received 15 July 2020 | Accepted 1 December 2020 | Published 20 January 2021

Letter

We still do not know when, where and how life started to exist on Earth. As the unique source of direct information about past life, the ancient fossil record may provide answers. Yet, although the ancient fossil record may contain fundamentally important 'biogeochemical' signals, its quality is far from perfect, making it not that easy to decode (Brasier *et al.*, 2006; Javaux, 2019). Archean palaeontology only relies on degraded signals difficult to interpret, as illustrated by the number of controversies having so far hindered the search for the most ancient traces of life on Earth (Schopf, 1975; Javaux, 2019).

A main difficulty is the lack of a univocal criterion to rely on when discussing the biogenicity of putative remains of life in ancient rocks: neither the carbon isotopic compositions nor the morphologies should be seen as unambiguous biosignatures (Craig, 1954; Horita, 2005; Cosmidis and Templeton, 2016; Garcia-Ruiz *et al.*, 2020). In fact, mineral biomorphs may easily be produced experimentally *via* self-assembly processes (Garcia-Ruiz *et al.*, 2003) and may exhibit high levels of complexity (Garcia-Ruiz *et al.*, 2009; Noorduin *et al.*, 2013; Rouillard *et al.*, 2018). Worse still, Cosmidis and Templeton (2016) recently demonstrated that carbon-sulfur biomorphs could also be produced.

Chemical information may help to identify remains of life (Benzerara *et al.*, 2006; Bernard *et al.*, 2007; Alleon *et al.*, 2018; Loron *et al.*, 2019), but abiotic processes may lead to the formation of disordered carbonaceous materials difficult to distinguish from biogenic ones (Pasteris and Wopenka, 2003; De Gregorio *et al.*, 2011). Collectively, because none of the criteria commonly used to discuss biogenicity are sufficient in themselves, many authors have emphasised the need for gathering multiple lines of evidence to demonstrate convincingly the biological origin of any putative remain of life in ancient cherts (*e.g.*, Westall, 2005; Wacey, 2009; Bernard and Papineau, 2014; Javaux, 2019). Yet, as illustrated by the present study, purely abiotic microstructures may fulfill not only a couple but many (if not all) of the commonly used criteria of biogenicity, *i.e.* morphological, chemical and isotopic criteria, even the most conservative ones (*cf.* below).

Here, we exposed RNA (*i.e.* the most emblematic organic molecule of the prebiotic RNA World; Higgs and Lehman, 2015) to thermal conditions typical of diagenesis (200 °C), in pure bi-distilled water under an autogenic pressure of 15 bars, in the presence of quartz (*i.e.* the main mineral of Archean cherts; Perry and Lefticariu, 2007) and under an argon atmosphere for 20 days. We conducted additional experiments under the same conditions with RNA in the absence of quartz and with quartz in the absence of RNA to serve as controls. The water insoluble experimental residues were characterised using X-ray diffraction (XRD), isotopic ratio mass spectrometry (IRMS), solid-state ^{13}C cross polarization magic-angle spinning nuclear magnetic resonance (^{13}C CP MAS NMR) and Fourier transform infrared (FTIR) spectroscopies. Additional characterisation was conducted using advanced microscopy and spectroscopy tools including scanning electron microscopy (SEM) coupled with energy dispersive X-ray spectroscopy (EDXS), scanning transmission electron microscopy (STEM) and scanning transmission X-ray microscopy (STXM) coupled with X-ray absorption near edge structure (XANES) spectroscopy.

1. Muséum National d'Histoire Naturelle, Sorbonne Université, CNRS UMR 7590, Institut de Minéralogie, Physique des Matériaux et Cosmochimie, Paris, France
2. Laboratoire d'Archéologie Moléculaire et Structurale, CNRS UMR 8220, Institut des Matériaux de Paris, Sorbonne Université, F-75005, Paris, France
* Corresponding author (email: sbernard@mnhn.fr)

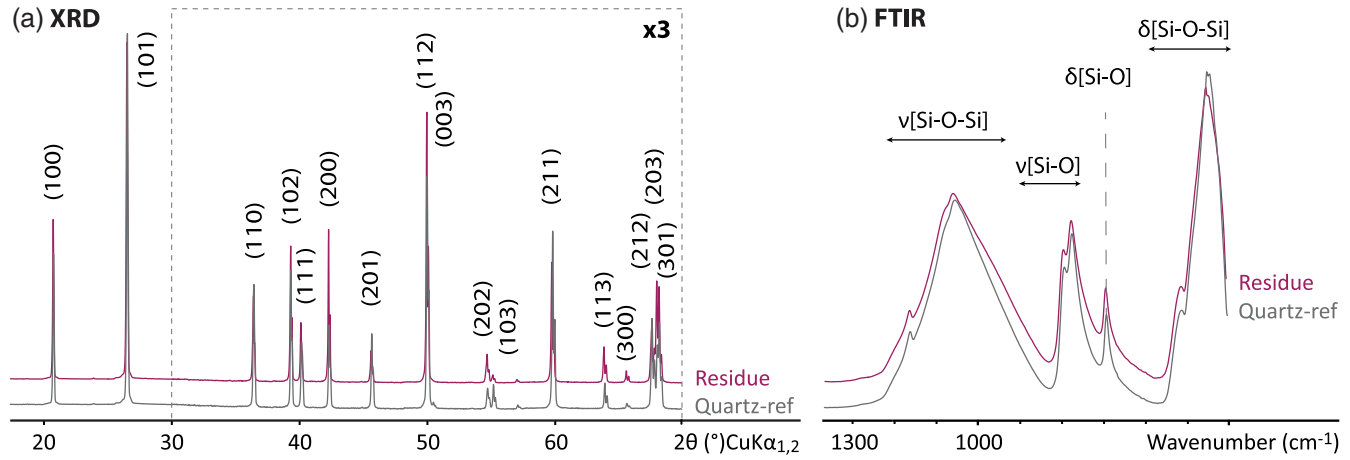

Figure 1 XRD and FTIR results. **(a)** Powder XRD patterns of the experimental residue (α-quartz + RNA + H_2O at 200 °C, 15 bars, 20 days) and of the α-quartz reference (intensity increased ×3 from 30 to 70° 2θ). **(b)** ATR-FTIR spectra of the experimental residue (α-quartz + RNA + H_2O at 200 °C, 15 bars, 20 days) and of the α-quartz reference.

Quartz was relatively unaffected by the experimental conditions. The main peaks of the XRD pattern of the experimental residue are those of α-quartz (*i.e.* 4.47 Å (100), 3.40 Å (101) and 2.57 Å (110); Fig. 1a). Likewise, the FTIR spectrum of the residue exhibits absorption bands typical of α-quartz (Fig. 1b): Si-O-Si and Si-O bending vibrations at 455 cm^{-1}, 514 cm^{-1} and 694 cm^{-1}, Si-O stretching vibrations at 775 and 794 cm^{-1} and Si-O-Si stretching vibrations at 1052 and 1160 cm^{-1} (Fig. 1b; Anbalagan *et al.*, 2010). Nevertheless, SEM images reveal the presence of dissolution pits at the surface of quartz grains, indicating that a certain fraction of quartz dissolved during the experiment (Fig. 2a).

Most importantly, SEM images show the presence, at the surface of the quartz grains, of newly formed spheroidal carbonaceous microstructures (Fig. 2), resembling micro-organisms such as *Staphylococcus* or *Thermococcales* (Fig. 2i,j). Arranged in clusters, these spheroidal organic biomorphs exhibit a rather restricted range of diameters of about ~0.5 to ~5 µm (µ = 2.03 µm; Fig. 2c). Most display a rough surface resembling the ultrastructure of living cells, and many are connected together as if they were microbes encompassing cell division (Fig. 2). These spheroidal organic biomorphs exhibit N/C values of 0.1 (*vs.* 0.4 for RNA), $\delta^{13}C$ values of −19.35 ± 0.04 ‰ (*vs.* −22.62 ± 0.04 ‰ for RNA) and $\delta^{15}N$ values of −9.95 ± 0.09 ‰ (*vs.* −12.11‰ ± 0.09 ‰ for RNA), *i.e.* values not that different from those expected for organic microfossils (*e.g.*, Craig, 1954; Mojzsis *et al.*, 1996; Horita, 2005).

While the NMR spectrum of RNA is dominated by the signals of ribose (between 60 and 105 ppm) and nucleobases (between 140 and 170 ppm), the NMR spectrum of these spheroidal organic biomorphs indicates the presence of aliphatic, aromatic and heterocyclic carbons (signals from 0 to 50 ppm, 100 to 130, and 130 to 150 ppm respectively) and amide and ketone groups (features at ~170 and 200 ppm) (Fig. 3a; Jacquemot *et al.*, 2019). This is in line with the FTIR spectrum showing C-H bending vibrations at 1367 cm^{-1}, aromatic C=C stretching vibrations at 1442 cm^{-1} and CH_3/CH_2 stretching vibrations from 2850 to 2980 cm^{-1} (Fig. 3b). The additional features at 1594 cm^{-1} and 1675 cm^{-1} highlight the presence of N-H bonds in amides or amines, as well as C=N bounds in imines or C=O bounds in ketones (Fig. 3b; Li *et al.*, 2014; Bernard *et al.*, 2015).

In contrast to RNA which C-XANES spectrum exhibits a number of well defined absorption features attributed to nucleobases and ribose (Fig. 4; Viennet *et al.*, 2019, 2020), the spheroidal organic biomorphs display a XANES spectrum with large features attributed to (hetero)quinones and olefinic or aromatic carbons (284.8–285.5 eV), imines, nitriles, ketones and/or phenols (286.4 eV) and amide groups (288.2 eV) (Fig. 4; Le Guillou *et al.*, 2018), *i.e.* a spectrum not that different from those expected for microfossils. The N-XANES spectrum confirms the presence of imine/nitrile (peaks at 398.3 and 399.4 eV) and amide functions (feature at 401.5 eV) (Fig. 4; Alleon *et al.*, 2017). Control experiments revealed that the presence of quartz has no influence on the properties of the produced spheroidal organic biomorphs (Fig. S-1).

By analogy with the production of hydrothermal carbon spheres (a.k.a. hydrochars), it can be assumed that the formation of these spheroidal organic biomorphs resulted from a cascade of reactions involving hydrolysis, dehydration, aromatisation and condensation (LaMer, 1952; Sevilla and Fuertes, 2009a,b). The entire process should not be seen as a suite of consecutive reactions, but rather as a parallel network of different reaction paths (Funke and Ziegler, 2010; Hu *et al.*, 2010). The hydrolysis of RNA likely produced organic acids having accelerated dehydration and fragmentation processes (*i.e.* ring opening and bond breaking), forming soluble by-products such as furfural-like compounds (Sevilla and Fuertes, 2009a,b). These by-products likely underwent aromatisation and condensation (possibly *via* intermolecular dehydration), leading to the production of aromatic clusters (Sevilla and Fuertes, 2009a,b). Burst nucleation processes likely took place when the concentration of aromatic clusters reached the critical supersaturation point, the nuclei growing by diffusion to the surface of the chemical species present in the solution, eventually forming the spheroidal organic biomorphs (Sevilla and Fuertes, 2009a,b). According to the LaMer model (LaMer, 1952), the structure of these spheroidal organic biomorphs should be composed of an aromatic-rich hydrophobic core and a hydrophilic surface containing a larger concentration of reactive oxygen-rich functional groups, as observed for hydrochars (Baccile *et al.*, 2009; Sevilla and Fuertes, 2009a,b; Higgins *et al.*, 2020). Yet, spatially resolved STXM investigations reveal that the spheroidal organic biomorphs produced here are quite homogeneous chemically, at least at the submicrometre scale, with rather equivalent concentrations of aromatic, ketone and amide groups inside their core and at their surface.

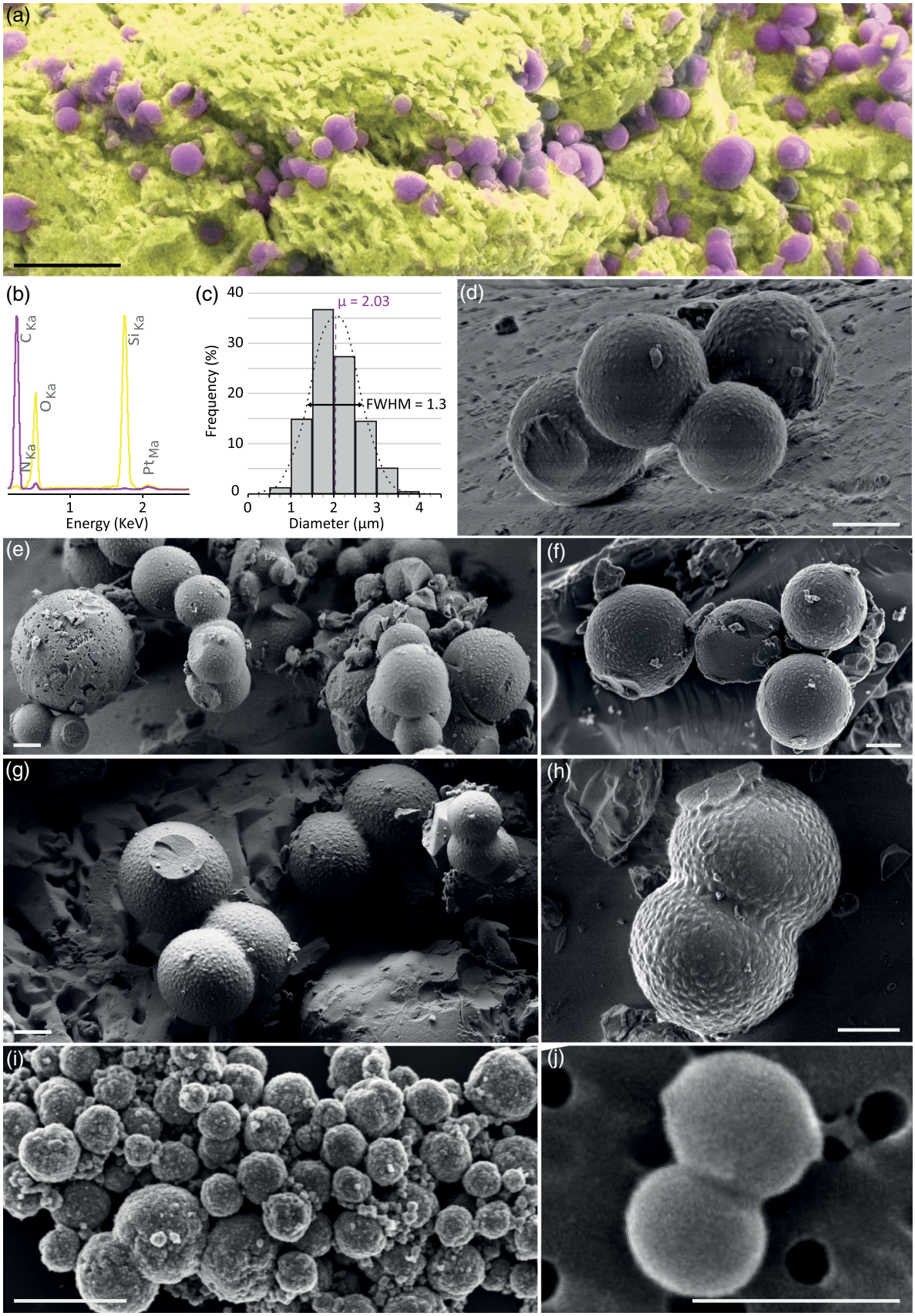

Figure 2 SEM investigations of the experimental residue (α-quartz + RNA + H_2O at 200 °C, 15 bars, 20 days). **(a)** EDX map of the residue and **(b)** corresponding EDX spectra. Quartz appears in yellow and the spheroidal organic biomorphs appear in purple. **(c)** Bar chart showing the size distribution of the spheroidal organic biomorphs produced during the experiments (FWHM: full width at half maximum). **(e-h)** SEM images (secondary electrons) of the spheroidal organic biomorphs produced during the experiments. **(f, g)** SEM images (secondary electrons) of *Thermococcus prieurii* cells (courtesy of Aurore Gorlas). Scale bars: **(a)** 10 μm, **(d-j)** 1 μm.

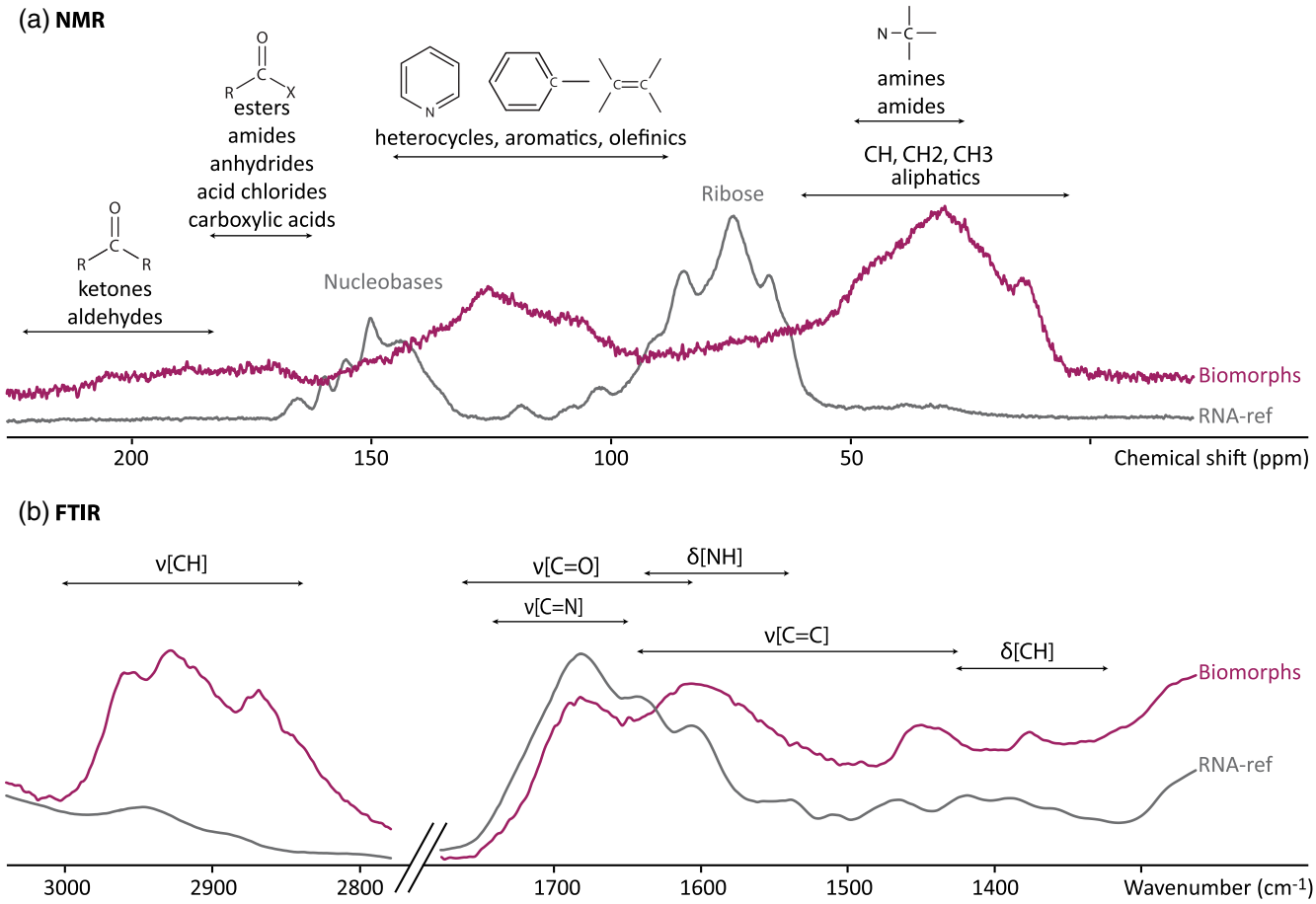

Figure 3 Solid state ^{13}C NMR and ATR-FTIR results. **(a)** Solid state ^{13}C CP MAS NMR spectra of the experimental residue (α-quartz + RNA + H_2O at 200 °C, 15 bars, 20 days) and of the RNA reference. Spectra are normalised to the quantity of carbon. **(b)** ATR-FTIR spectra of the experimental residue (α-quartz + RNA + H_2O at 200 °C, 15 bars, 20 days) and of the RNA reference. Spectra are normalised to the total carbon content. Note that the intensity of the signals were increased ×3 for clarity from ~3035 to ~2775 cm^{-1}.

Collectively, in contrast to mobile hydrocarbon microspheres that can be encountered in the geological record (Wanger *et al.*, 2012), the spheroidal organic biomorphs produced here exhibit all the morphological and geochemical features typical of organic microfossils (size, morphology, ultrastructure, chemistry, isotopic signatures). Worse still, it has been shown that, if exposed to pressure and temperature conditions typical of the geological history undergone by ancient cherts, such spheroidal organic biomorphs may evolve into double shell hollow spheres (Hu *et al.*, 2010; Li *et al.*, 2016). In other words, because they meet all the criteria commonly used to discuss biogenicity, even the most conservative ones (Brasier *et al.*, 2006), the abiotic spheroidal organic biomorphs described here would logically be recognised as truly biogenic organic microfossils if they were found in ancient cherts.

The results of the present study exemplify the pitfalls that Archean palaeontologists may encounter when searching for traces of life in ancient rocks (*e.g.*, Schopf, 1975; Javaux, 2019). It is clear that if new strategies are not adopted, ambiguities and controversies will persist. Advanced spatially resolved spectroscopy techniques may provide some clues regarding the molecular structure of putative organic microfossils (*e.g.*, Brasier *et al.*, 2015; Alleon and Summons, 2019), but this is not sufficient. Because unambiguously determining the exact nature of putative organic microfossils requires information on their original chemical nature, only laboratory experiments may provide the necessary constraints to eventually decode the most ancient fossil record (*e.g.*, Javaux, 2019).

Author Contributions

IC, PJ and SB designed the present study. IC and PJ performed the NMR analyses. IC, PJ and SB performed the SEM analyses. IC and JCV performed the EA-IRMS analyses, the XRD analyses and the FTIR analyses. IC, JCV and SB performed the STXM analyses. All authors contributed to the interpretation of the data and discussed their implications. IC, JVC and SB wrote the manuscript, with critical inputs from PJ and MJ.

Acknowledgements

We acknowledge the support of the MNHN and of the IMPMC spectroscopy platform. We thank Elisabeth Malassis (IMPMC) for administrative support, Aurore Gorlas (I2BC) for SEM images of *Thermococcus prieurii* cells, Imène Esteve (IMPMC) for her help with SEM, Etienne Balan (IMPMC) for his help with FTIR, Denis Fiorillo (AASPE) for his help with EA-IRMS, Baptiste Rigaud (IMPC) for his help with NMR, David Troadec (IEMN) for the preparation of FIB sections, Corentin Le Guillou (UMET) for the TEM image and Sufal Swaraj (Soleil) for the expert support of the HERMES STXM beamline

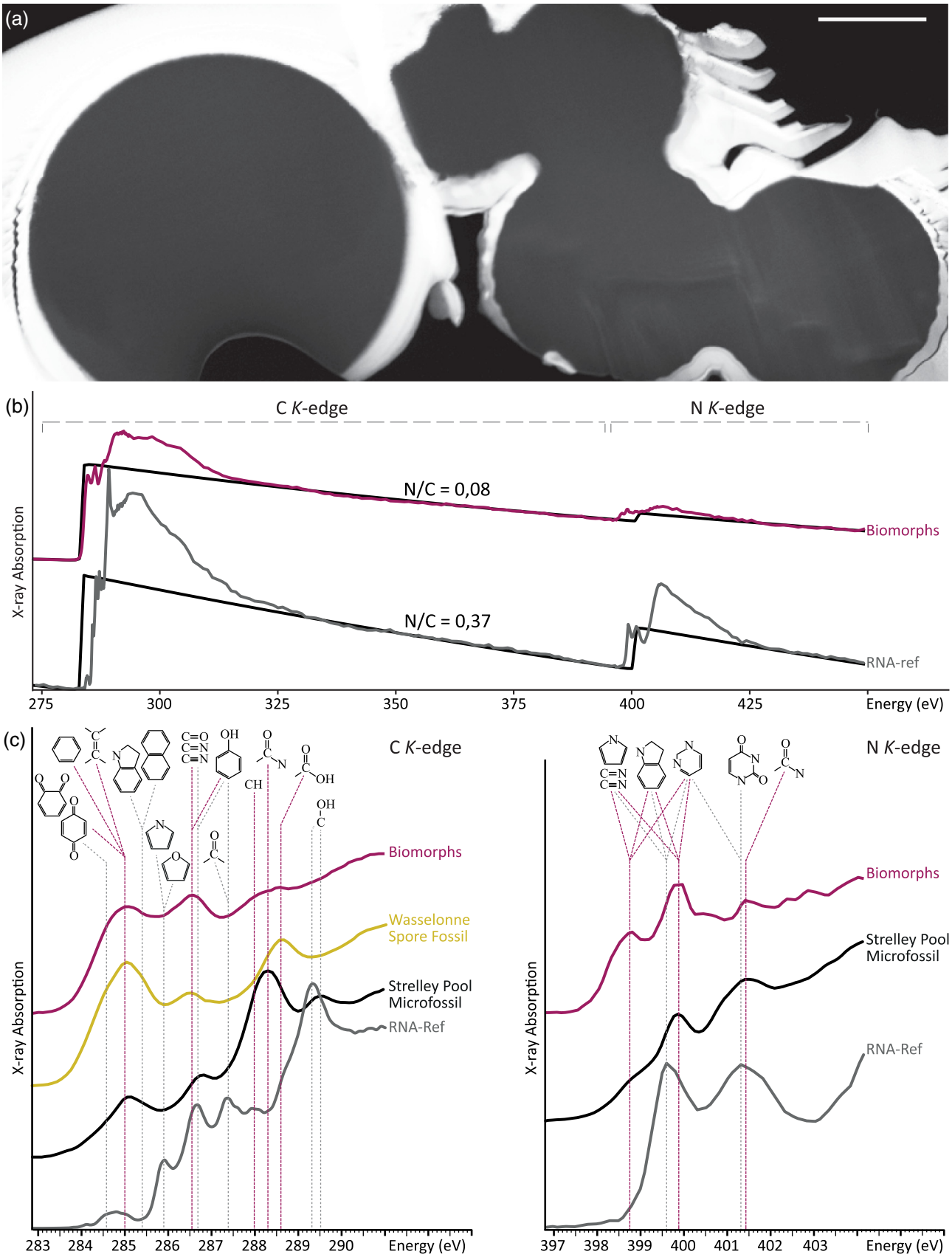

Figure 4 STEM and STXM-XANES results. **(a)** Transmission electron microscopy image (STEM mode) of the FIB section extracted from spheroidal organic biomorphs. Scale bar: 1µm. **(b)** X-Ray absorption spectra of the organic biomorphs and of the RNA reference, with their corresponding N/C values. **(c)** C- and N-XANES spectra of the organic biomorphs and of the RNA reference compared to spectra of organic microfossils from Wasselonne (Bernard *et al.*, 2009) and Strelley Pool (Alleon *et al.*, 2018). All spectra are normalised to C and N quantities.

at SOLEIL. The SEM facility at IMPMC is supported by Region Ile de France grant SESAME Number I-07-593/R, INSU-CNRS, INP-CNRS and UPMC-Paris 6, and by the Agence Nationale de la Recherche (ANR) grant number ANR-07-BLAN-0124-01. The TEM facility at the CCM (Lille University) is supported by the Chevreul Institute, the European FEDER, and Région Nord-Pas-de-Calais. The HERMES beamline (SOLEIL) is supported by the CNRS, the CEA, the Region Ile de France, the Departmental Council of Essonne and the Region Centre.

Editor: Satish Myneni

Additional Information

Supplementary Information accompanies this letter at https://www.geochemicalperspectivesletters.org/article2102.

Cite this letter as: Criouet, I., Viennet, J.-C., Jacquemot, P., Jaber, M., Bernard, S. (2021) Abiotic formation of organic biomorphs under diagenetic conditions. *Geochem. Persp. Let.* 16, 40–46.

References

Anbalagan, G., Prabakaran, A., Gunasekaran, S. (2010) Spectroscopic characterization of Indian standard sand. *Journal of Applied Spectroscopy* 77, 86–94.

Alleon, J., Bernard, S., Le Guillou, C., Daval, D., Skouri-Panet, F., Kuga, M., Robert, F. (2017) Organic molecular heterogeneities can withstand diagenesis. *Scientific Reports* 7, 1508.

Alleon, J., Bernard, S., Le Guillou, C., Beyssac, O., Sugitani, K., Robert, F. (2018) Chemical nature of the 3.4 Ga Strelley Pool microfossils. *Geochemical Perspectives Letters* 7, 37–42.

Alleon, J., Summons, R.E. (2019) Organic geochemical approaches to understanding early life. *Free Radical Biology and Medicine* 140, 103–112.

Baccile, N., Laurent, G., Babonneau, F., Fayon, F., Titirici, M.-M., Antonietti, M. (2009) Structural Characterization of Hydrothermal Carbon Spheres by Advanced Solid-State MAS ^{13} C NMR Investigations. *The Journal of Physical Chemistry C* 113, 9644–9654.

Benzerara, K., Menguy, N., Lopez-Garcia, P., Yoon, T.-H., Kazmierczak, J., Tyliszczak, T., Guyot, F., Brown, G.E. (2006) Nanoscale detection of organic signatures in carbonate microbialites. *Proceedings of the National Academy of Sciences* 103, 9440–9445.

Bernard, S., Papineau, D. (2014) Graphitic Carbons and Biosignatures. *Elements* 10, 435–440.

Bernard, S., Benzerara, K., Beyssac, O., Menguy, N., Guyot, F., Brownjr, G., Goffe, B. (2007) Exceptional preservation of fossil plant spores in high-pressure metamorphic rocks. *Earth and Planetary Science Letters* 262, 257–272.

Bernard, S., Benzerara, K., Beyssac, O., Brown, G.E., Stamm, L.G., Duringer, P. (2009) Ultrastructural and chemical study of modern and fossil sporoderms by Scanning Transmission X-ray Microscopy (STXM). *Review of Palaeobotany and Palynology* 156, 248–261.

Bernard, S., Benzerara, K., Beyssac, O., Balan, E., Brown Jr., G.E. (2015) Evolution of the macromolecular structure of sporopollenin during thermal degradation. *Heliyon* 1, e00034.

Brasier, M., McLoughlin, N., Green, O., Wacey, D. (2006) A fresh look at the fossil evidence for early Archaean cellular life. *Philosophical Transactions of the Royal Society B: Biological Sciences* 361, 887–902.

Brasier, M.D., Antcliffe, J., Saunders, M., Wacey, D. (2015) Changing the picture of Earth's earliest fossils (3.5–1.9 Ga) with new approaches and new discoveries. *Proceedings of the National Academy of Sciences* 112, 4859–4864.

Cosmidis, J., Templeton, A.S. (2016) Self-Assembly of biomorphic carbon/sulfur microstructures in sulfidic environments. *Nature Communications* 7, 12812.

Craig, H. (1954) Geochemical implications of the isotopic composition of carbon in ancient rocks. *Geochimica et Cosmochimica Acta* 6, 186–196.

De Gregorio, B.T., Sharp, T.G., Rushdi, A.I., Simoneit, B.R.T. (2011) Bugs or Gunk? Nanoscale Methods for Assessing the Biogenicity of Ancient Microfossils and Organic Matter. In: Golding, S.D., Glikson, M. (Eds.) *Earliest Life on Earth: Habitats, Environments and Methods of Detection*. Springer Netherlands, Dordrecht, 239–289.

Funke, A., Ziegler, F. (2010) Hydrothermal carbonization of biomass: A summary and discussion of chemical mechanisms for process engineering. *Biofuels, Bioproducts and Biorefining* 4, 160–177.

Garcia-Ruiz, J.M., Hyde, S.T., Carnerup, A.M., Christy, A.G., Van Kranendonk, M.J., Welham, N.J. (2003) Self-Assembled Silica-Carbonate Structures and Detection of Ancient Microfossils. *Science* 302, 1194–1197.

Garcia-Ruiz, J.M., Melero-Garcia, E., Hyde, S.T. (2009) Morphogenesis of Self-Assembled Nanocrystalline Materials of Barium Carbonate and Silica. *Science* 323, 362–365.

Garcia-Ruiz, J.M., van Zuilen, M.A., Bach, W. (2020) Mineral self-organization on a lifeless planet. *Physics of Life Reviews* 34–35, 62–82.

Higgins, L.J.R., Brown, A.P., Harrington, J.P., Ross, A.B., Kaulich, B., Mishra, B. (2020) Evidence for a core-shell structure of hydrothermal carbon. *Carbon* 161, 423–431.

Higgs, P.G., Lehman, N. (2015) The RNA World: molecular cooperation at the origins of life. *Nature Reviews Genetics* 16, 7–17.

Horita, J. (2005) Some perspectives on isotope biosignatures for early life. *Chemical Geology* 218, 171–186.

Hu, B., Wang, K., Wu, L., Yu, S.-H., Antonietti, M., Titirici, M.-M. (2010) Engineering Carbon Materials from the Hydrothermal Carbonization Process of Biomass. *Advanced Materials* 22, 813–828.

Jacquemot, P., Viennet, J.C., Bernard, S., Le Guillou, C., Rigaud, B., Delbes, L., Georgelin, T., Jaber, M. (2019) The degradation of organic compounds impacts the crystallization of clay minerals and vice versa. *Scientific Reports* 9, 20251.

Javaux, E.J. (2019) Challenges in evidencing the earliest traces of life. *Nature* 572, 451–460.

LaMer, V.K. (1952) Nucleation in Phase Transitions. *Industrial & Engineering Chemistry* 44, 1270–1277.

Le Guillou, C., Bernard, S., De la Pena, F., Le Brech, Y. (2018) XANES-Based Quantification of Carbon Functional Group Concentrations. *Analytical Chemistry* 90, 8379–8386.

Li, J., Bernard, S., Benzerara, K., Beyssac, O., Allard, T., Cosmidis, J., Moussou, J. (2014) Impact of biomineralization on the preservation of microorganisms during fossilization: An experimental perspective. *Earth and Planetary Science Letters* 400, 113–122.

Li, S., Pasc, A., Fierro, V., Celzard, A. (2016) Hollow carbon spheres, synthesis and applications – a review. *Journal of Materials Chemistry A* 4, 12686–12713.

Loron, C.C., François, C., Rainbird, R.H., Turner, E.C., Borensztajn, S., Javaux, E.J. (2019) Early fungi from the Proterozoic era in Arctic Canada. *Nature* 570, 232–235.

Mojzsis, S.J., Arrhenius, G., McKeegan, K.D., Harrison, T.M., Nutman, A.P., Friend, C.R.L. (1996) Evidence for life on Earth before 3,800 million years ago. *Nature* 384, 55–59.

Noorduin, W.L., Grinthal, A., Mahadevan, L., Aizenberg, J. (2013) Rationally Designed Complex, Hierarchical Microarchitectures. *Science* 340, 832–837.

Pasteris, J.D., Wopenka, B. (2003) Necessary, but Not Sufficient: Raman Identification of Disordered Carbon as a Signature of Ancient Life. *Astrobiology* 3, 727–738.

Perry, E.C., Lefticariu, L. (2007) Formation and Geochemistry of Precambrian Cherts. *Treatise on Geochemistry* 7, 1–21.

Rouillard, J., García-Ruiz, J.-M., Gong, J., van Zuilen, M.A. (2018) A morphogram for silica-witherite biomorphs and its application to microfossil identification in the early earth rock record. *Geobiology* 16, 279–296.

Schopf, J.W. (1975) Precambrian Paleobiology: Problems and Perspectives. *Annual Review of Earth and Planetary Sciences* 3, 213–249.

Sevilla, M., Fuertes, A.B. (2009a) Chemical and Structural Properties of Carbonaceous Products Obtained by Hydrothermal Carbonization of Saccharides. *Chemistry – A European Journal* 15, 4195–4203.

Sevilla, M., Fuertes, A.B. (2009b) The production of carbon materials by hydrothermal carbonization of cellulose. *Carbon* 47, 2281–2289.

Viennet, J.-C., Bernard, S., Le Guillou, C., Jacquemot, P., Balan, E., Delbes, L., Rigaud, B., Georgelin, T., Jaber, M. (2019) Experimental clues for detecting biosignatures on Mars. *Geochemical Perspectives Letters* 12, 28–33.

Viennet, J.-C., Bernard, S., Le Guillou, C., Jacquemot, P., Delbes, L., Balan, E., Jaber, M. (2020) Influence of the nature of the gas phase on the degradation of RNA during fossilization processes. *Applied Clay Science* 191, 105616.

Wacey, D. (Ed.) (2009) *Early Life on Earth*. Springer Netherlands, Dordrecht.

Wanger, G., Moser, D., Hay, M., Myneni, S., Onstott, T.C., Southam, G. (2012) Mobile hydrocarbon microspheres from >2-billion-year-old carbon-bearing seams in the South African deep subsurface. *Geobiology* 10, 496–505.

Westall, F. (2005) Early Life on Earth: The Ancient Fossil Record. In: Ehrenfreund, P., Irvine, W.M., Owen, T., Becker, L., Blank, J., Brucato, J.R., Colangeli, L., Derenne, S., Dutrey, A., Despois, D., Lazcano, A., Robert, F. (Eds.) *Astrobiology: Future Perspectives*. Springer Netherlands, Dordrecht, 287–316.

Geochemical Perspectives Letters

Abiotic formation of organic biomorphs under diagenetic conditions

I. Criouet, J.C. Viennet, P. Jacquemot, M. Jaber, S. Bernard

Supplementary Information

The Supplementary Information includes:

- Methods
- Figure S-1
- Supplementary Information References

Methods

Experimental procedure

Pure powder of yeast RNA and α-quartz (Sigma-Aldrich) were used for the present experiments. 100 mg of RNA and 200 mg of α-quartz were mixed within 5 mL of pure bi-distilled water and introduced in a PTFE reactor (Parr) filled by pure argon (> 99.99 %) in a glove box. These reactors were placed in a MEMMERT UN30 oven at 200 °C for 20 days. The soluble fraction of the experimental residues was extracted by centrifugation and the remaining solid fraction was then washed 3 times with pure bi-distilled water and dried overnight in an oven at 50 °C before characterisation.

SEM, FIB & STEM

Scanning electron microscopy (SEM) investigations were performed on powders deposited on carbon tape using a SEM-FEG ZEISS ULTRA 55 (IMPMC, Paris) equipped with a Bruker EDS QUANTAX detector (Bruker Corporation, Houston, TX, USA). Images shown here (secondary electrons) were collected using an acceleration voltage below 2 kV, thereby preventing irradiation damages. Electron dispersive X-ray spectroscopy (EDXS) maps were collected on powders coated with 5 nm of platinum using an acceleration voltage of 10 kV. Focused ion beam (FIB) foils were extracted from organic biomorphs never exposed to high acceleration voltage using an FEI Strata DB 235 (IEMN, Lille, France). Milling at low gallium ion currents allowed minimising common artefacts including local gallium implantation, mixing of components, redeposition of the sputtered material on the sample surface and significant changes in the speciation of carbon-based polymers (Bernard *et al.*, 2009; Schiffbauer and Xiao, 2009). Transmission electron microscopy in scanning mode (STEM) was performed on the FIB foils using a Thermofisher Titan Themis 300 microscope operated at 300 keV (CCM – Lille, France).

Size distribution

The area of a thousand of biomorphs was measured on SEM images using the ImageJ elliptical selection tool. The equivalent diameter of each biomorph was estimated such as $d_{eq} = 2\sqrt{(Area/\pi)}$ (Rouillard *et al.*, 2018).

EA-IRMS

Total carbon and nitrogen contents and C and N isotopic compositions were determined using a Flash 2000 Thermo CHNSO elemental analyser coupled to a Thermo Fisher DeltaV Advantage IRMA (MNHN SSMIM, Paris). Experimental residues were primarily flash combusted at 1020 °C in the oxidation column of the EA (chromium oxide, cobaltous oxide, quartz wool). Oxidation products were then carried by a stream of helium (100 mL/min) through the reduction column (copper, quartz wool) at 650 °C and water was removed from the resulting gases through a magnesium perchlorate filter. The CO_2 and N_2 were then separated in a chromatographic column heated at 40 °C, passed through a thermal conductivity detector (1000 µV) where elemental compositions were measured, and carried into the source of the IRMS where the isotope ratios were measured. Alanine was used as standard for both elemental and isotopic analyses and for uncertainties.

XRD

X-Ray diffraction (XRD) patterns were acquired using a BRUKER D2 PHASER diffractometer (IMPMC, Paris) operating at 30 kV and 10 mA with a Cu anode ($K\alpha_{1,2}$ at 1.54 Å). Analyses were performed on finely ground powders deposited on a silicium sample holder. The angular range in 2θ was 5-70° with a step size of 0.03° and with a counting time of 3 s per step.

NMR & FTIR

Cross polarisation ^{13}C nuclear magnetic resonance (NMR) experiments were performed with a magic-angle spinning probe 1H/X at 14000 kHz using a BRUKER AVANCE III 500 MHz (IMPC, Paris) operating at 125.77 MHz. Chemical shifts were calibrated using the carboxyl signal of adamantane (38.52 ppm). NMR data were acquired with a contact time of 1 ms and a recycle delay of 1.5 s. Note that this configuration only provides qualitative information, especially as the possible presence of radical species may be responsible for quenching of signals. Fourier-transform infrared (FTIR) spectra were recorded in the 400-4000 cm^{-1} range with a 4 cm^{-1} resolution using a Nicolet 6700 FTIR spectrometer fitted with a KBr beamsplitter and a DTGS-KBr detector. The powder spectra were obtained under ambient conditions by averaging 200 scans obtained in attenuated total reflectance (ATR) geometry using a Specac Quest ATR device fitted with a diamond internal reflection element.

STXM-based XANES

Scanning transmission X-ray microscopy (STXM) analyses were performed on FIB foils to document both the carbon and nitrogen speciation of the biomorphs using the HERMES STXM beamline at the synchrotron SOLEIL (Saint-Aubin, France - Belkhou *et al.*, 2015; Swaraj *et al.*, 2017). Energy calibration was done using the well-resolved 3p Rydberg peak of gaseous CO_2 at 294.96 eV for the C K-edge, and using the $1s \rightarrow \pi^*$ photoabsorption resonance of gaseous N_2 at 400.8 eV for the N K-edge. X-ray absorption near edge structure (XANES) hypercube data (stacks) were collected with a spatial resolution of 35 nm at energy increments of 1 eV over the 250-450 eV region and at energy increments of 0.1 eV over the carbon (270–340 eV) and the nitrogen (390–450 eV) absorption ranges with a dwell time of less than 1 ms per pixel to prevent irradiation damage (Wang *et al.*, 2009). Stack alignments and extraction of XANES spectra were done using the aXis2000 software. Normalisation of data was done using the QUANTORXS freeware (Le Guillou *et al.*, 2018).

Supplementary Figure

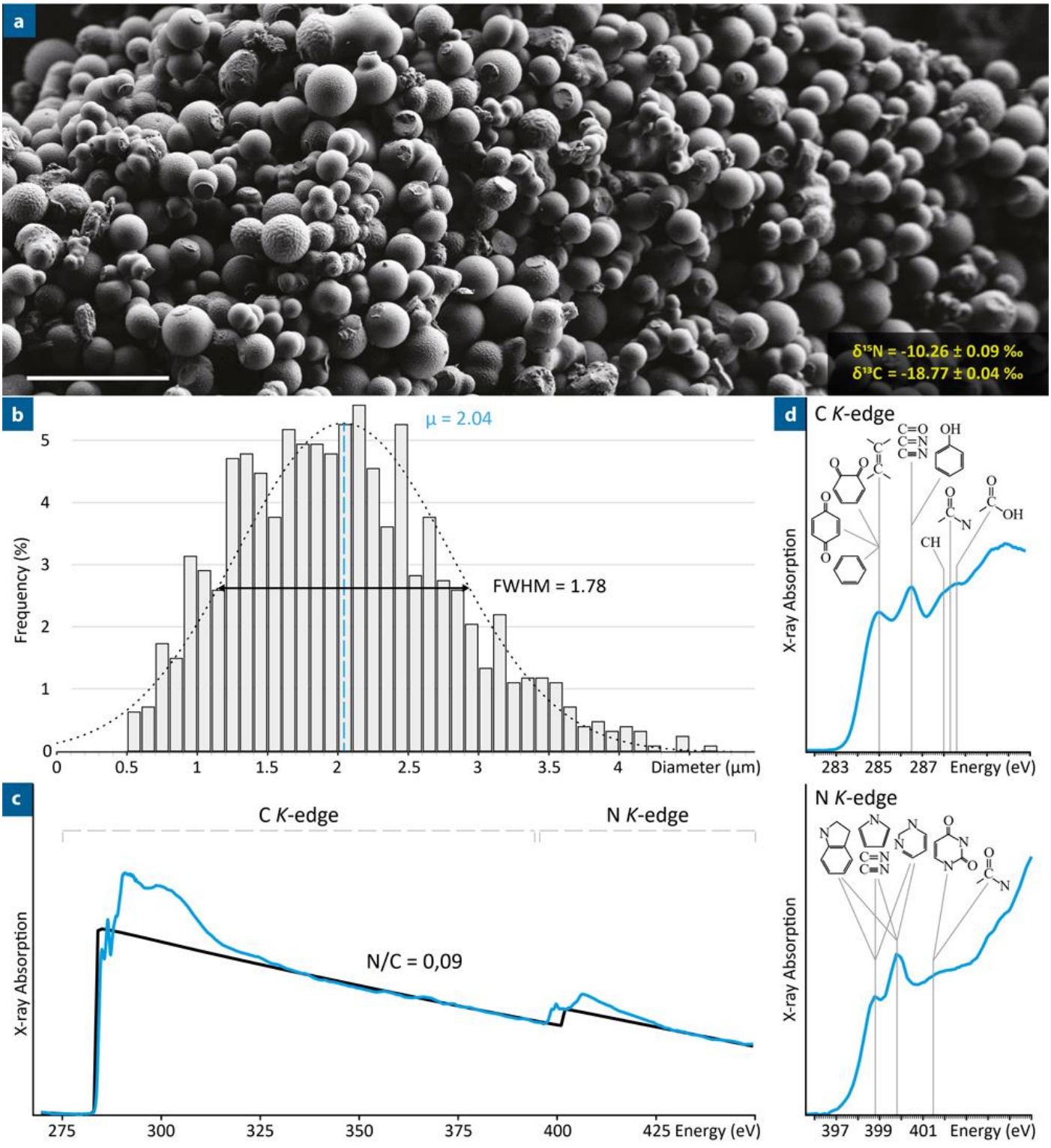

Figure S-1 Results of the quartz-free control experiment. **(a)** SEM image (secondary electrons) of the organic biomorphs produced in the absence of quartz. Their $\delta^{13}C$ and $\delta^{15}N$ are indicated in yellow. Scale bar: 10 µm. **(b)** Bar chart showing the size distribution of the spheroidal organic biomorphs produced in the absence of quartz (FWHM: full width at half maximum). **(c)** X-ray absorption spectrum of the spheroidal organic biomorphs produced in the absence of quartz and their corresponding N/C value. **(d)** C- and N-XANES spectra of the spheroidal organic biomorphs produced in the absence of quartz

Supplementary Information References

Belkhou, R., Stanescu, S., Swaraj, S., Besson, A., Ledoux, M., Hajlaoui, M., Dalle, D. (2015) HERMES: a soft X-ray beamline dedicated to X-ray microscopy. *Journal of Synchrotron Radiation* 22, 968–979.

Bernard, S., Benzerara, K., Beyssac, O., Brown, G.E., Stamm, L.G., Duringer, P. (2009) Ultrastructural and chemical study of modern and fossil sporoderms by Scanning Transmission X-ray Microscopy (STXM). *Review of Palaeobotany and Palynology* 156, 248–261.

Le Guillou, C., Bernard, S., De la Pena, F., Le Brech, Y. (2018) XANES-Based Quantification of Carbon Functional Group Concentrations. *Analytical Chemistry* 90, 8379–8386.

Rouillard, J., García-Ruiz, J.-M., Gong, J., van Zuilen, M.A. (2018) A morphogram for silica-witherite biomorphs and its application to microfossil identification in the early earth rock record. *Geobiology* 16, 279–296.

Schiffbauer, J.D., Xiao, S. (2009) Novel application of focused ion beam electron microscopy (FIB-EM) in preparation and analysis of microfossil ultrastructures: A new view of complexity in early Eukaryotic organisms. *PALAIOS* 24, 616–626.

Swaraj, S., Belkhou, R., Stanescu, S., Rioult, M., Besson, A., Hitchcock, A.P. (2017) Performance of the HERMES beamline at the carbon K-edge. *Journal of Physics: Conference Series* 849, 012046.

Wang, J., Morin, C., Li, L., Scholl, A., Doran, A. (2009) Radiation damage in soft X-ray microscopy. *Journal of Electron Spectroscopy and Related Phenomena* 170, 25–36.

.